Geophysical Research Letters

RESEARCH LETTER
10.1029/2022GL098086

Key Points:

- P wave radial anisotropic structure beneath the young and highly extended Woodlark rift is constrained from teleseismic tomography
- Downwelling of slab relics bordering the rift zone may contribute to ultra-high pressure rock exhumation and rift development
- Slab-pull drives rift initiation and induces decompression melting in the upper mantle under the rift zone by horizontal stress transfer

Supporting Information:

Supporting Information may be found in the online version of this article.

Correspondence to:

Y. Yu,
yuyouqiang@tongji.edu.cn

Citation:

Yu, Y., Tilmann, F., Zhao, D., Gao, S. S., & Liu, K. H. (2022). Continental break-up under a convergent setting: Insights from P wave radial anisotropy tomography of the Woodlark rift in Papua New Guinea. *Geophysical Research Letters*, *49*, e2022GL098086. https://doi.org/10.1029/2022GL098086

Received 26 JAN 2022
Accepted 24 FEB 2022

Continental Break-Up Under a Convergent Setting: Insights From P Wave Radial Anisotropy Tomography of the Woodlark Rift in Papua New Guinea

Youqiang Yu[1,2,3], Frederik Tilmann[2,4], Dapeng Zhao[5], Stephen S. Gao[3], and Kelly H. Liu[3]

[1]State Key Laboratory of Marine Geology, Tongji University, Shanghai, China, [2]GFZ German Research Centre for Geosciences, Potsdam, Germany, [3]Geology and Geophysics Program, Missouri University of Science and Technology, Rolla, MO, USA, [4]Institute for Geological Sciences, Freie Universität Berlin, Berlin, Germany, [5]Department of Geophysics, Graduate School of Science, Tohoku University, Sendai, Japan

Abstract To explore the dynamic mechanism of continental rifting within a convergent setting, we determine the first P wave radial anisotropic tomography beneath the Woodlark rift in southeastern Papua New Guinea, which develops within the obliquely colliding zone between the Australian and southwest Pacific plates. The rift zone is depicted as localized low-velocity anomalies with positive radial anisotropy, which rules out a dominant role of active mantle upwelling in promoting the rift development and favors passive rifting with decompression melting as main processes. Downwelling slab relics in the upper mantle bounding the rift zone are revealed based on observed high-velocity anomalies and negative radial anisotropy, which may contribute to the ultra-high pressure rock exhumations and rift initiation. Our observations thus indicate that the Woodlark rift follows a passive model and is mainly driven by slab pull from the northward subduction of the Solomon plate.

Plain Language Summary The Woodlark rift in Papua New Guinea develops within the shear zone between the Australian and southwest Pacific plates and is one of the youngest and most rapidly extending continental rifts in the world. In this work, we analyze teleseismic P wave arrivals to study both 3-D velocity and radial anisotropy structures of the upper mantle, offering new evidence to understand rift initiation under a generally convergent setting. Slab remnants in the upper mantle bordering the rift zone are detected and sinking into the deeper mantle. Downwelling of these slab segments may induce small scale return flows in the mantle and contribute to exhumation of the ultra-high pressure rocks and rift development. Significant low-velocity anomalies are revealed beneath the rift zone and have consistently positive radial anisotropy, which indicates a dominant strain in the horizontal plane and supports a passive rifting model, where mantle material is brought to shallower depths simply as a result of the extension of the lithosphere and melt is produced due to the lowered melting point at reduced pressure (decompression melting). Tensional stresses transferred from slab pull of the northward Solomon subduction are probably driving the rifting.

1. Introduction

Rifting represents the initial stage of the breakup of continents and ultimately leads to the formation of passive margins and oceanic lithosphere, which is usually driven by active mantle upwelling or far-field extensional stresses (Sengör & Burke, 1978). Extensive studies have been conducted on slow, intracontinental rifts such as the East African rift system within the African plate and the Baikal rift inside the Eurasian plate (e.g., Adams et al., 2018; Chorowicz, 2005; Gao et al., 1994), while rift initiation under a generally convergent tectonic setting, where a compositionally quite heterogeneous lithosphere is commonly involved, remains a topic of intense investigation. The Woodlark rift in southeastern Papua New Guinea lies within an obliquely and rapidly (~110 mm/yr) convergent boundary zone between the Australian and Pacific plates, which is accommodated by a complex array of microplates in between (Tregoning et al., 1998; Wallace et al., 2004). This area offers a rare glimpse of active rift propagation (Figure 1) from seafloor spreading of the Woodlark basin in the east to initial continental breakup in the west (Eilon et al., 2014; Taylor et al., 1999). The Woodlark rift behaves as one of the youngest (<8.3 Ma) and most rapidly extending (10–15 mm/yr) continental rifts in the world (e.g., Taylor & Huchon, 2002, Taylor et al., 1999; Wallace et al., 2004, 2014).

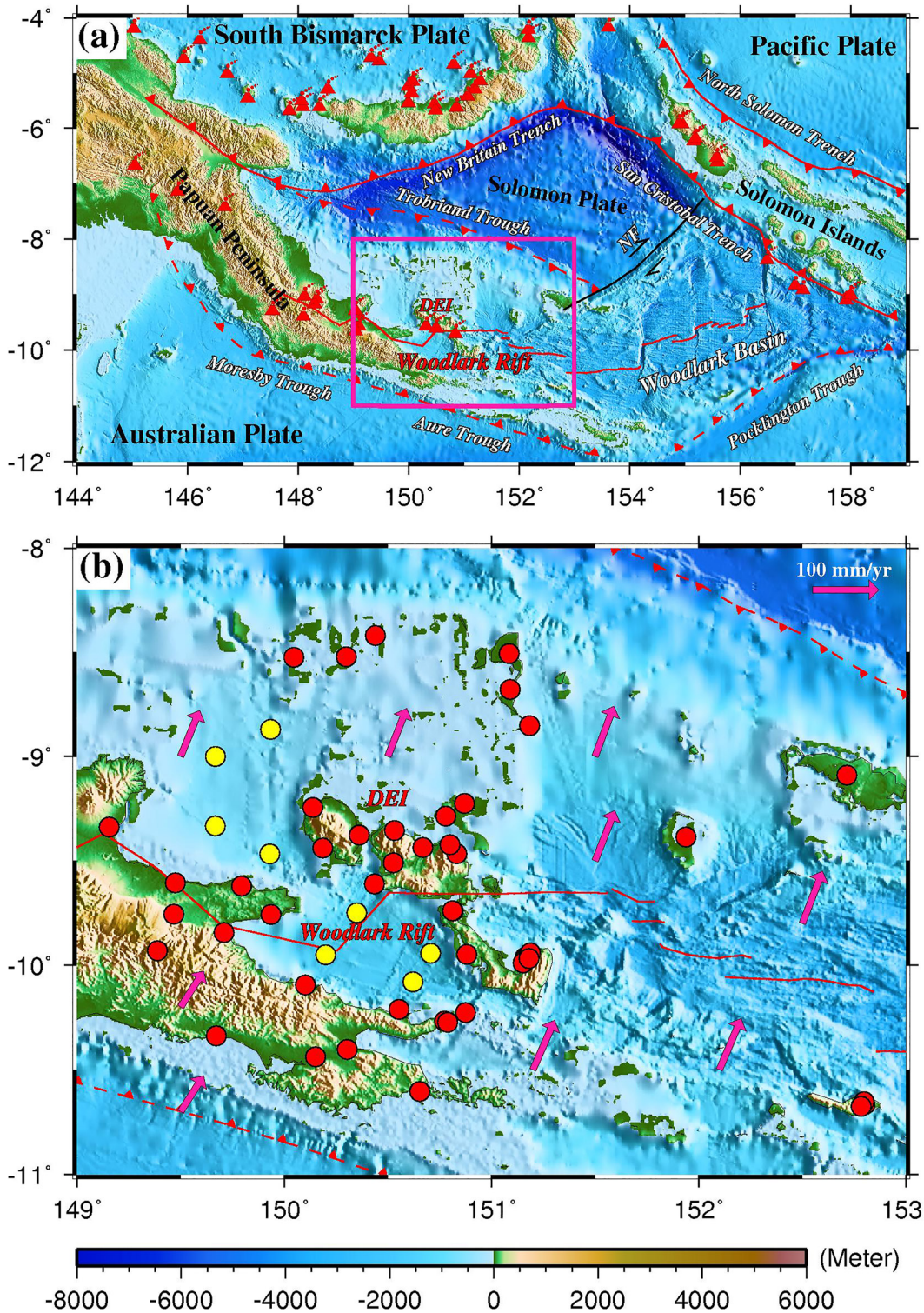

Figure 1. (a) Tectonic setting of southeastern Papua New Guinea. The purple rectangle highlights the study area. Red lines depict the axis of the seafloor spreading center and continental break-up. Solid and dashed red toothed lines represent currently active and past subductions, respectively. Volcanic centers are plotted as red triangles. D'Entrecasteaux Islands (DEI); Nubara Fault (NF). (b) Distribution of the broadband seismic stations used in this study (color dots). Red and yellow dots denote on-land and ocean bottom seismograph stations, respectively. Purple arrows show the absolute plate motion directions from the NNR-MORVEL56 model (Argus et al., 2011).

The Woodlark rift separates the Australian margins from the Woodlark microplates. During the Paleogene to early Miocene, the northern Australian rifted passive margin subducted beneath an island arc terrane with some Australian plate rocks possibly brought into mantle depths (Davies & Jaques, 1984; Lus et al., 2004; Smith & Davies, 1976). A short-period of southward subduction of the Solomon Sea plate existed along the Trobriand Trough in the Early Miocene (Taylor & Huchon, 2002). Since the late Miocene, northward subduction of the Solomon Sea plate along the New Britain trench, which is instigated by the continuous oblique convergence between the Pacific and Australian plates (Figure 1), produced a strong slab-pull force to cause counterclockwise rotations of the Woodlark and Solomon Sea microplates relative to the Australian plate about nearby Euler poles to the southwest (Biemiller et al., 2020; Wallace et al., 2014). Such microplate rotations have possibly initiated north-south seafloor spreading within the Woodlark basin since about 6 Ma as deciphered by magnetic anomalies (Taylor et al., 1999) and promoted continental rifting within the Woodlark rift (Hall, 2002; Weissel et al., 1982). The active Woodlark basin is currently subducting beneath the Solomon island arc along its northeastern margin (Figure 1). Metamorphic core complexes are rapidly exhumed at the Papuan Peninsula and the D'Entrecasteaux Islands (DEI) near the center of the Woodlark rift where the youngest (Late Miocene-Pliocene) known ultra-high pressure (UHP) eclogitic rocks on Earth are hosted, possibly linked to the rifting (e.g., Baldwin et al., 2004; Eilon et al., 2015; Gordon et al., 2012; Little et al., 2011; Webb et al., 2008).

Most of current understandings on the crust and mantle structures beneath the Woodlark rift are from a series of seismological studies mainly based on analysis of data from seismic experiments WOODSEIS (Abers et al., 2002; Ferris et al., 2006) and CDPapua (Eilon et al., 2014). The crust of the rift zone is revealed to have thinned by 10–15 km and possess felsic bulk compositions, and the higher topography beneath the DEI was proposed to be compensated by a low-density, low-velocity upper mantle (Abers et al., 2002, 2016; Ferris et al., 2006). A narrow E-W corridor of significant low-velocity anomalies (LVAs) extending from the crust to a mantle depth of about 250 km is revealed along the rift axis from both Rayleigh-wave (Jin et al., 2015) and body-wave (Eilon et al., 2015, 2016) tomography, and has been interpreted as lithospheric removal due to mantle divergence and adiabatic upwelling. In addition, a recently combined global and regional tomography model suggests that hot buoyant material from a cryptic mantle plume has been upwelling through slab remnants and contributed to volcanism in Northern Australia and New Guinea (B. L. N. Kennett & Davies, 2020). However, both shear wave splitting and azimuthal anisotropic body wave tomography studies based on data from CDPapua experiment present strong azimuthal anisotropy in the upper mantle beneath the rift zone with dominantly spreading-parallel fast orientations, which favors horizontal mantle flow and is similar to what observed at a mid-ocean ridge (Eilon et al., 2014, 2016). Whether the observed LVAs beneath the rift zone correspond to a regime of active mantle upwelling or passive melting in response to rifting extension thus remains unclear. Here, we explore the region's radial anisotropy structure in order to further discriminate between these hypotheses.

Radial anisotropy, also defined as polarization anisotropy or vertical transverse isotropy, provides an effective way to discriminate the dominant strain between the vertical and horizontal planes, which further helps constrain the vertical tectonic regime. Lattice-preferred orientation of anisotropic minerals such as olivine is proposed to be the major mechanism of generating the detected seismic anisotropy in the upper mantle (Silver, 1996) and the observed radial anisotropy is used to characterize the difference between the horizontal and vertical velocities. Specifically, negative (vertical velocity is faster than horizontal velocity) and positive radial anisotropies usually depict the vertical and horizontal mantle flows, respectively. In this study, we use all the available broadband seismic data in the Woodlark rift accumulated so far to jointly investigate the 3-D P-wave velocity (Vp) and radial anisotropy structures by systematically conducting radial anisotropy tomography, which offers new constraints on the mechanism of continental rift development within an overall convergent tectonic background.

2. Data and Methods

All the broadband seismic data used in this study were requested from the Incorporated Research Institutions for Seismology Data Management Center and recorded at a total of 59 stations (Figure 1) among which 19 stations were deployed by the WOODSEIS experiment (network of XD, Abers et al., 2002; Ferris et al., 2006) and 40 stations belong to the CDPapua experiment (network of ZN, Eilon et al., 2014). The 19 stations of network XD have a recording time between July 1999 and June 2000, and the network ZN comprises 32 on-land stations and 8 OBSs (ocean bottom seismographs) operating from March 2010 to July 2011. Time correction has been conducted for all the OBS data with more details found in Eilon et al. (2014). Teleseismic events (hypocentral parameters

from United States Geological Survey) with a minimum magnitude of 4.5, epicentral distances 25°–95° and recorded at 5 or more stations, were considered for analysis. After visual inspection for quality control, all teleseismic P wave arrivals were manually picked on the original vertical-component seismograms (Figure S1 in the Supporting Information S1), with an estimated picking accuracy of ∼0.1–0.2 s (Yu et al., 2017). As a result, we have obtained 10,503 P wave arrivals from 795 teleseismic events (Figure S2 in the Supporting Information S1) for the final tomographic inversion. Travel time residuals were computed with respect to the IASP91 theoretical travel times (Kennett & Engdahl, 1991). The CRUST1.0 model (Laske et al., 2013) was employed to compensate for the lateral variations of crustal structure. To minimize the influence of hypocentral mislocation and velocity heterogeneities outside the modeling volume (Zhao et al., 1994), relative travel-time residuals were computed by subtracting the average residual for each event and mostly fall in a range of −1–+1 s (Figure S3 in the Supporting Information S1). Significant delayed arrivals are revealed to be generally distributed within the rift zone based on the resulting station-averaged relative travel-time residuals (Figure S4 in the Supporting Information S1).

We firstly arrange a 3-D grid with a lateral interval of 0.5° and vertical intervals of 40–70 km in the depth range of 50–340 km, and then apply the tomographic method of Zhao et al. (1994) to determine a 3-D isotropic Vp model of the upper mantle beneath the study region based on the relative travel-time residuals, which aims to estimate the resolution just for the isotropic tomography. Then, 3-D isotropic Vp and radial anisotropy are jointly inverted for using the updated technique of Wang and Zhao (2013), which incorporates two sets of 3-D grids: a fine grid with intervals as described above for the isotropic Vp model, and a coarse grid with a lateral grid interval of 0.8° and at depths of 50, 130 and 220 km for the Vp radial anisotropy parameter (percent anisotropy); positive and negative radial anisotropies indicate faster velocities in the horizontal and vertical directions, respectively. The two grids are necessary as the radial anisotropy inversion requires better ray coverage per node. Vp perturbations at any point in the model are calculated by bicubic interpolation (Zhao et al., 1992). The ray paths for a given station-event pair are efficiently traced by combining the pseudo-bending algorithm and Snell's law (Zhao et al., 1992). Most of the study area (especially the rift zone) at each depth is well sampled by the rays (Figures S5–S7 in the Supporting Information S1). The use of relative travel times implies that only lateral differences can be resolved; this is true both for the isotropic perturbations and the radial anisotropy parameter.

A critical quantity for the resolvability of radial anisotropy is the variability of incidence angles. For teleseismic P arrivals at 25°–95° epicentral distance, as are exclusively used here, incidence angles i vary between ∼15° and ∼30° in the upper mantle. As partial derivatives are proportional to cos (2i) (Wang & Zhao, 2013, their Equation 9), this limited angular range nevertheless results in significant variation of partial derivatives with incidence angle which allows to resolve radial anisotropy structure at coarse scale, as we will demonstrate below with resolution tests (Section 3). We adopt the iterative conjugate-gradient LSQR algorithm (Paige & Saunders, 1982) with damping and smoothing regularizations (Zhao et al., 1994) to solve the large and sparse system of resulting equations. Although the optimal damping and smoothing parameters are determined independently for both isotropic Vp and Vp radial anisotropy, the optimal parameters turn out to be 40 for damping and 0.0012 for smoothing in each case, based on the tradeoff curves (Figure S8 in the Supporting Information S1) between the root-mean-square (RMS) travel time residual and the norm of the 3-D Vp model. The RMS travel-time residual is reduced from 0.503 to 0.344 s and 0.341 s after the isotropic and anisotropic tomography inversions, respectively (Figure S3 in the Supporting Information S1).

3. Resolution Tests

The spatial resolutions of the tomographic models are evaluated by conducting a series of checkerboard resolution tests (CRTs) with different lateral grid intervals and extensive synthetic tests (Figures S9–S28 in the Supporting Information S1). We use the location parameters of all the stations and events from the real data to compute synthetic travel time residuals for a given input 3-D model. To simulate the picking errors in the observed data, random noise (−0.2–+0.2 s) with a standard deviation of 0.1 s (Zhao et al., 1992) is added to the synthetic data, which are then inverted for a 3-D output model based on the same tomography methods. Positive and negative Vp anomalies of 4% are alternatively added to the 3-D grid nodes to generate the isotropic checkerboard input model. We have selected three representative sets of grid intervals (0.3°, 0.5° and 0.7°, note that the parametrization is set according to the grid interval) to conduct CRTs (Figures S9–S11 in the Supporting Information S1). The test results suggest that our isotropic Vp model has a lateral resolution of 0.5° and a depth resolution of ∼50 km. The main features of the tomographic images are further confirmed by conducting a restoring resolution test (RRT)

with an input model derived from the tomographic results (Figures S12 and S13 in the Supporting Information S1). The smearing effect is also investigated by adopting an input model including high and low Vp anomalies that extend to different depths (Figures S14 and S15 in the Supporting Information S1). Similar procedures are adopted to evaluate the radial anisotropy tomography with the addition of alternatively positive and negative radial anisotropy (±2%) assigned to the coarse grid nodes, while retaining the isotropic checkerboard pattern (Figures S16–S18 in the Supporting Information S1). We also examined the trade-off between the isotropic Vp and radial anisotropy by setting either isotropic Vp anomalies or the anisotropic parameters as zero in the input model (Figures S19 and S20 in the Supporting Information S1). The coupling between isotropic Vp and radial anisotropy (Huang et al., 2015) is also evaluated by conducting RRTs and also assigning the input high-velocity anomalies (HVAs) with either positive or negative radial anisotropy (Figures S21-S28 in the Supporting Information S1). All these synthetic tests show that both the isotropic Vp and anisotropy results over most of the study area are robust, especially for the Woodlark rift zone.

4. Results and Discussion

4.1. Downwelling of Slab Relics and Ultra-High Pressure Rock Exhumation

Several prominent features are revealed in the resulting velocity and anisotropy tomography images (Figures 2 and 3). The dominant structure is the low-velocity rift zone being sandwiched by HVAs to the north and south (Figure S29 in the Supporting Information S1). And most of the major HVAs are characterized by an overwhelming negative radial anisotropy (Figures 2, 3 and S30 in the Supporting Information S1). The southern HVA is continuous from ∼130 to 220 km depth. In comparison, the northern HVA, which appears to comprise two distinct parts, is most prominent in the shallower mantle at depths from 50 to 90 km and gradually diminishes below, disappearing completely below 170 km. An isolated HVA is found in the northwest of the study region at 340 km depth. These HVAs may correspond to lithospheric fragments, either from delamination of continental lithosphere or are relic slabs from subduction zones active in the past, specifically those associated with the Trobriand trough just north of the study area and the Aure, Moresby and Pocklington troughs to the south and east (Figure 1). Prominent HVAs north of the rift axis were also seen from earlier isotropic inversions of teleseismic P and S arrivals and were interpreted as relic slab fragments; this interpretation is supported by the occurrence of intermediate-depth seismicity inside this HVA (Abers et al., 2016; Eilon et al., 2015, 2016). Rayleigh-wave tomography from both ambient noise and earthquake signals also detected localized HVAs bounding the flanks of the rift zone in the uppermost mantle (Jin et al., 2015). The presence of adakitic melts northwest of the rift zone is also consistent with this interpretation, as those melts are derived from partial melting of remnant mafic eclogite and/or garnet-amphibolite, that is, remnants of oceanic crust (Haschke & Ben-Avraham, 2005). In addition, the arc-type volcanics with calc-alkaline basaltic to rhyolitic composition across the Papuan Peninsula and the persistence of mantle relief beneath the DEI were proposed to have resulted from melting of an inferred underlying Trobriand subducted slab (e.g., Little et al., 2011; Martinez et al., 2001; Stolz et al., 1993). The Solomon plate was postulated to subduct southwards at the Trobriand Trough from the early Miocene (possibly late Oligocene) through the late Miocene, but this subduction process is thought to have stalled with the onset of northward subduction of the same plate at New Britain and the San Cristobal trenches (e.g., Benes et al., 1994; Fitz & Mann, 2013; Martinez & Taylor, 1996; Smith & Davies, 1976; Taylor & Huchon, 2002; Wallace et al., 2014). The existence of the southward subduction of the Solomon plate at the Trobriand Trough is favored in a proposed physical model to explain low-angle normal faulting in the Woodlark extensional province (Westaway, 2005) and further supported by a recent plate kinematic model (Benyshek & Taylor, 2021). The cessation of the southward subduction would make the subducted Solomon slab sink and progressively pull the slab into a steeper angle, which has been proposed to be a viable mechanism for explaining lower crustal thinning in the absence of upper crust deformation (e.g., Fitz & Mann, 2013; Kington & Goodliffe, 2008). The steepened slab remnants may be characterized as the northern HVA. Geochemical and geological observations (Cloos et al., 2005; Holm et al., 2015; Pigram et al., 1989; Webb et al., 2014) indicate that a short-lived episode of northward subduction (Figure 4) was ongoing along the Aure-Moresby and Pocklington Troughs during the Eocene (or younger), followed by slab break-off. Fragments of this slab could still be found in the upper mantle and explain the southern HVA. Thus, the observed HVAs bordering the rift zone in the upper mantle most likely represent slab relics from the past subductions.

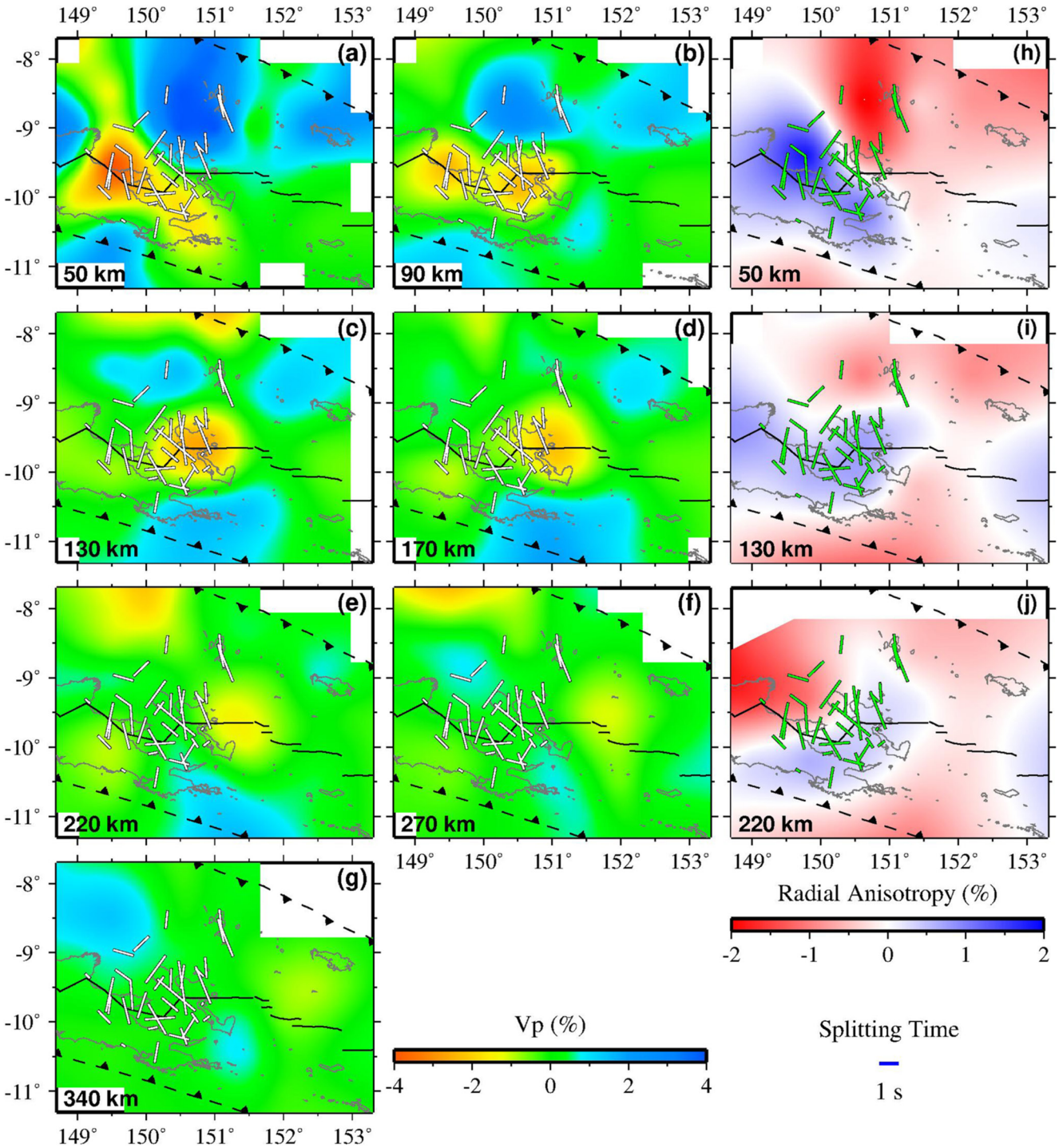

Figure 2. Map views of resulting isotropic Vp (a–g) and radial anisotropy (h–j) at different depths as shown at the lower-left corner of each map. The white and green bars display fast orientations of shear-wave splitting measurements (Eilon et al., 2014). Gray and black lines indicate coastlines and rift axis, respectively. Dashed black toothed lines represent inactive trenches.

The observed negative radial anisotropy of the HVAs may indicate a downwelling motion (Figure 4) similar to what is observed beneath Southern California (Yu & Zhao, 2018), the Central Anatolian Plateau (Göğüş et al., 2017) and central Tibet (Zhang et al., 2016). Lithospheric downwelling can be triggered by a density contrast of as little as 1% based on numerical studies of the Great Basin (West et al., 2009). Given the relatively high viscosity of relic slab, gravitational pull from the lower part of these slab remnants would stretch the

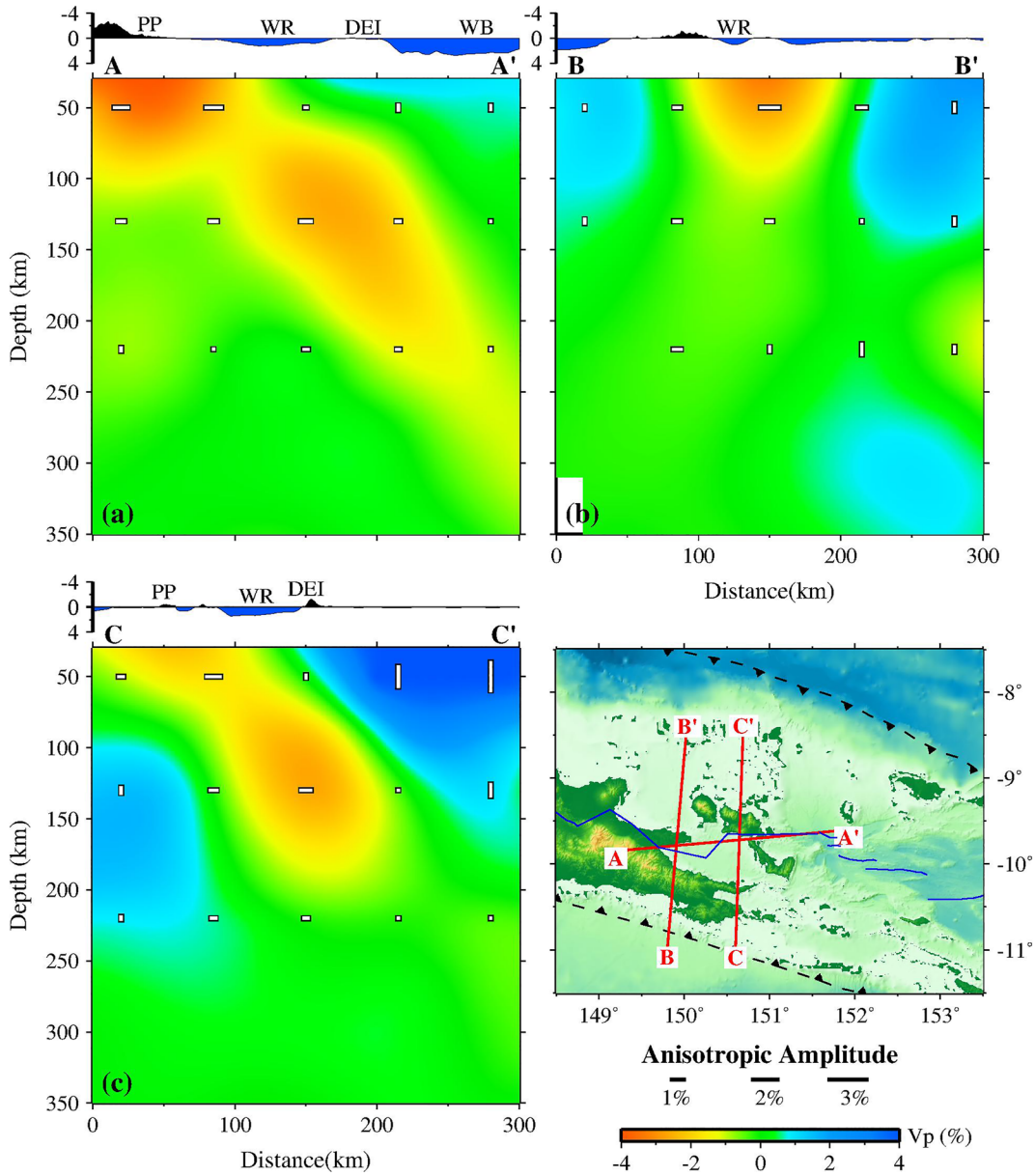

Figure 3. Vertical cross-sections of isotropic Vp (colors) and radial anisotropy (white bars) along the three profiles on the inset map. The vertical and horizontal white bars represent faster velocity in the vertical and horizontal directions, respectively. The bar length denotes the strength of radial anisotropy. Papuan Peninsula (PP); Woodlark basin (WB); Woodlark rift (WB).

lithospheric fabrics vertically by pure shear and thus also align the fast crystallographic axis vertically, generating negative radial anisotropy. Such a mechanism has been proposed to explain the formation of cratonic roots based on global surface-wave tomography (Priestley et al., 2021). In addition, slab steepening may tilt the fossil fabrics preserved within the slab from horizontal into vertical orientations, which partially contribute to the observed negative radial anisotropy.

It is noticeable that exposures of the UHP rocks, which have been extensively exhumed at the DEI in the last 8–4 Ma (Baldwin et al., 2004; Monteleone et al., 2007) mostly situate above the edges of the observed HVAs. Thermal-mechanical modeling and geodetic evidence are compatible with a diapir model, where the UHP rocks are derived from previously subducted continental fragment, which are exhumed via buoyancy forces (Ellis et al., 2011; Little et al., 2011; Wallace et al., 2014). The downwelling of the slab relics may in turn produce small

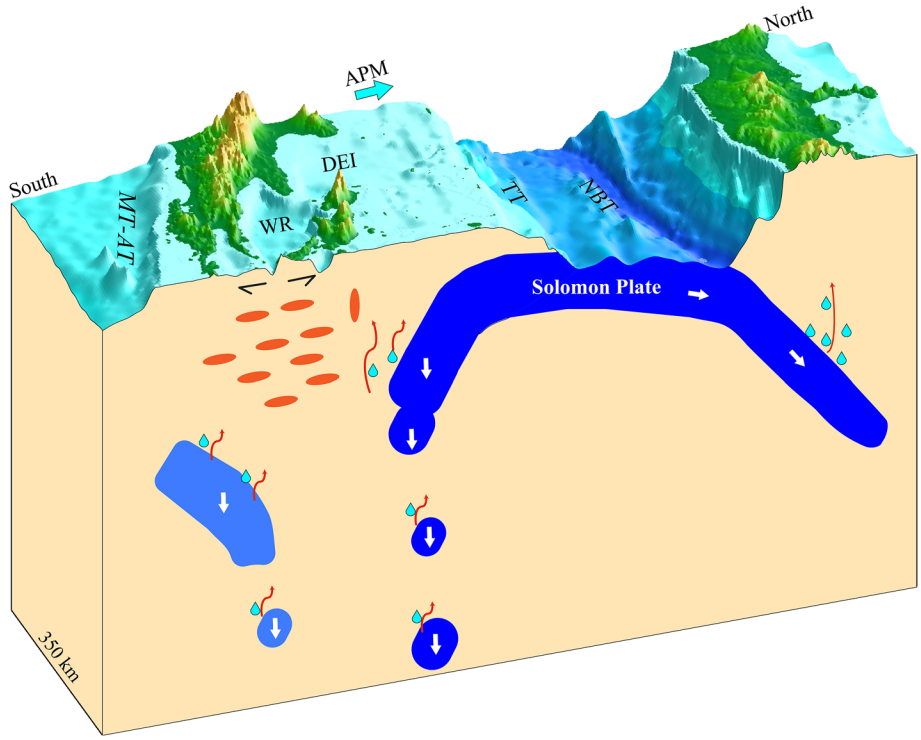

Figure 4. A conceptual diagram showing tectonics and subduction dynamics of the Woodlark rift. Absolute Plate Motion (APM); New Britain Trench (NBT), Moresby Trough-Aure Trough (MT-AT). The cyan drops denote dehydrated water. Red arrows indicate dehydration melting or small mantle upwelling associated with sinking of the slab segments. Orange ellipses represent decompression melting with their long axis displaying the dominant strain orientations.

pipes of mantle upwelling at their edges (Göğüş et al., 2017), leading to the generation of melts, which in turn can infiltrate and weaken the lithosphere above the remnant slabs (Figure 4). In addition, volatiles released from these slab relics may further weaken upper mantle and crust beneath the DEI (Kington & Goodliffe, 2008; Martinez et al., 2001), promoting exhumations of UHP rocks. Our observations suggest that the existence and downwelling of slab remnants may contribute to the exhumation of UHP rocks in addition to the rifting tectonics.

4.2. Decompression Melting Beneath the Rift Zone

Significant LVAs are revealed to mostly distribute along the rift axis with mostly prominent positive radial anisotropy (Figures 2 and 3). At less than 100 km, they appear as a LVA elongated in E-W direction, although an eastern and western limb can be distinguished. At 100–200 km, only the eastern limb remains, resulting in a circular anomaly in map view. The lack of a deep-seated low-velocity anomaly below 250 km rules out a dominant role of a potential deep mantle plume in driving the rift development. 3-D numerical modeling of the Woodlark basin also demonstrated that a mantle plume is not necessary for initiating and sustaining continental rifting (Mondy et al., 2018). The observation that LVAs reach a maximum depth of about 250 km near the seafloor spreading center in the east and become shallower westwards (Figure 3a) may indicate a westward propagation of mantle deformation in response to the extending rate. A similarly narrow LVA within the rift zone in the upper mantle was also imaged from body wave tomography based on data from the CDPapua passive seismic experiment (Eilon et al., 2015). Substantial crustal thinning and low sub-Moho velocities beneath the rift zone were likewise inferred from Rayleigh wave and receiver function inversions (Abers et al., 2002, 2016; Ferris et al., 2006; Jin et al., 2015). The observed positive radial anisotropy below the rift zone from our joint tomographic inversion (Figure 2) indicates a dominant strain in the horizontal plane (Figure 4), which is quite consistent with the strong spreading-parallel azimuthal anisotropy obtained from shear wave splitting analysis (Eilon et al., 2014) and shear wave anisotropy tomography (Eilon et al., 2016). Similar features have been detected beneath the Salton Trough, also developing under a convergent setting within the shear zone between the Pacific and North American plates (Yu & Zhao, 2018). In comparison, isolated mantle upwelling, characterized as localized LVAs with negative

radial anisotropy, was proposed to possibly contribute to lithospheric weakening at the early stage of intra-plate continental rifting based on results from the Malawi rift, which is a young rift segment of the East African rift system and develops under a divergent setting (Yu et al., 2020). The existence of mantle upwelling beneath the rift zone would usually lead to negative radial anisotropy and small/undetected azimuthal anisotropy, which is in conflict with both the radial anisotropy measurements from this study and the azimuthal anisotropy from Eilon et al. (2014, 2016). The lithospheric extension will lead to mantle material following upward trajectories, causing decompression melting in the upper mantle of the rift zone (Figure 4); the presence of small amounts of melts could explain the high Vp/Vs ratios observed by Eilon et al. (2015) and further lower velocities within the rift zone.

The Woodlark rift is currently developing within the obliquely convergent zone along the irregular boundary between the southwest Pacific and Indo-Australian plates. Geodetic data (Biemiller et al., 2020; Tregoning et al., 1998; Wallace et al., 2004, 2014) indicate that the northwards subduction of the Solomon plate has driven the Woodlark microplate to rotate anticlockwise away from the Australian plate. The north flank of the Woodlark rift is moving northward faster than its southern flank, implying north-south extension, and a tensional stress field in the lithosphere, which induces lithospheric stretching. The upward movement of asthenospheric mantle implied by this process can induce decompression melting, which leads to the observed LVAs and positive radial anisotropy beneath the rift zone (Figure 2). Rifting prefers to propagate along weak zones in the lithosphere (Van Wijk & Blackman, 2005) and the existence of neighboring rigid slab remnants might facilitate strain focusing (Eilon et al., 2015). In addition, dehydration of these slab segments would promote melting of the overlying mantle and contribute to the rift development (e.g., Fitz & Mann., 2013; Kington & Goodliffe, 2008; Martinez et al., 2001; Stolz et al., 1993). In general, the Woodlark rift seems to follow a passive model (Figure 4) in which plate motions resulting from the slab-pull force of the northward Solomon subduction play the dominant role, and its development is possibly influenced by slab relics from the past subductions.

5. Conclusions

In this study, we have developed the first 3-D model of P wave radial anisotropy tomography for the Woodlark rift by inverting all available teleseismic P wave travel time data accumulated so far. LVAs are mostly confined to the shallow upper mantle of the rift axis and display uniformly positive radial anisotropy, which is inconsistent with the existence of active mantle upwelling and favors decompression melting. The depth of the LVAs within the rift zone decrease westwards with a maximum value of about 250 km near the seafloor spreading center and is in close response to the westward rift propagation. HVAs with negative radial anisotropy are detected in the upper mantle at the north and south flanks of the rift zone and may denote a downwelling mechanism of slab relics from past subductions. The existence and downwelling of these slab remnants may contribute to the overlying mantle deformations possibly associated with the rift development and exhumation of ultra-high pressure rocks.

Data Availability Statement

All the data used in this study were downloaded from the Incorporated Research Institutions for Seismology Data Management Center (https://ds.iris.edu/ds/nodes/dmc/) with network codes including XD (https://doi.org/10.7914/SN/XD_1999) and ZN (https://doi.org/10.7914/SN/ZN_2010).

Acknowledgments
This study was funded by the National Natural Science Foundation of China (grant 42074052) and partially supported by the United States National Science Foundation (grant 1919789), the Alexander von Humboldt foundation, and Japan Society for the Promotion of Science (grant 19H01996). Prof. Lucy Flesch (the Editor) and two anonymous referees provided thoughtful review comments and suggestions, which have improved this paper.

References

Abers, G. A., Eilon, Z., Gaherty, J. B., Jin, G., Kim, Y.-S., Obrebski, M., & Dieck, C. (2016). Southeast Papuan crustal tectonics: Imaging extension and buoyancy of an active rift. *Journal of Geophysical Research: Solid Earth*, *121*, 951–971. https://doi.org/10.1002/2015JB012621

Abers, G. A., Ferris, A., Craig, M., Davies, H., Lerner-Lam, A. L., Mutter, J. C., & Taylor, B. (2002). Mantle compensation of a region of active metamorphic core complexes, Woodlark Rift, Papua New Guinea. *Nature*, *418*, 862–865. https://doi.org/10.1038/nature00990

Adams, A., Miller, J., & Accardo, N. (2018). Relationships between lithospheric structures and rifting in the east African rift system: A Rayleigh wave tomography study. *Geochemistry, Geophysics, Geosystems*, *19*, 3793–3810. https://doi.org/10.1029/2018GC007750

Argus, D. F., Gordon, R. G., & DeMets, C. (2011). Geologically current motion of 56 plates relative to the no-net-rotation reference frame. *Geochemistry, Geophysics, Geosystems*, *12*, Q11001. https://doi.org/10.1029/2011GC003751

Baldwin, S. L., Monteleone, B. D., Webb, L. E., Fitzgerald, P. G., Grove, M., & Hill, E. J. (2004). Pliocene eclogite exhumation at plate tectonic rates in eastern Papua New Guinea. *Nature*, *431*, 263–267. https://doi.org/10.1038/nature02846

Benes, V., Scott, S. D., & Binns, R. A. (1994). Tectonics of rift propagation into a continental margin: Western Woodlark basin, Papua New Guinea. *Journal of Geophysical Research*, *99*(B3), 4439–4455. https://doi.org/10.1029/93JB02878

Benyshek, E. K., & Taylor, B. (2021). Tectonics of the papua-woodlark region. *Geochemistry, Geophysics, Geosystems*, *22*, e2020GC009209. https://doi.org/10.1029/2020GC009209

Biemiller, J., Boulton, C., Wallace, L., Ellis, S., Little, T., Mizera, M., et al. (2020). Mechanical implications of creep and partial coupling on the world's fastest slipping low-angle normal fault in southeastern Papua New Guinea. *Journal of Geophysical Research: Solid Earth*, *125*(10), e2020JB020117. https://doi.org/10.1029/2020JB020117

Chorowicz, J. (2005). The East African rift system. *Journal of African Earth Sciences*, *43*, 379–410. https://doi.org/10.1016/j.jafrearsci.2005.07.019

Cloos, M., Sapiie, B., van Ufford, A. Q., Weiland, R. J., Warren, P. Q., & McMahon, T. P. (2005). Collisional Delamination in New Guinea: The Geotectonics of Subducting Slab Breakoff, Geological Society of America, (Vol. *400*, pp. 1–51). https://doi.org/10.1130/2005.2400

Davies, H. L., & Jaques, A. L. (1984). Emplacement of ophiolite in Papua New Guinea. In I. G. Gass, S. J. Lippar, & A. W. Shelton (Eds.), *Ophiolites and oceanic lithosphere*, (Vol. 13, pp. 341–350). Geological Society. https://doi.org/10.1144/gsl.sp.1984.013.01.27

Eilon, Z., Abers, A. A., & Gaherty, J. B. (2016). A joint inversion for shear velocity and anisotropy: The Woodlark Rift, Papua New Guinea. *Geophysical Journal International*, *206*, 807–824. https://doi.org/10.1093/gji/ggw177

Eilon, Z., Abers, G. A., Gaherty, J. B., & Jin, G. (2015). Imaging continental breakup using teleseismic body waves: The Woodlark Rift, Papua New Guinea. *Geochemistry, Geophysics, Geosystems*, *16*, 2529–2548. https://doi.org/10.1002/2015GC005835

Eilon, Z., Abers, G. A., Jin, G., & Gaherty, J. B. (2014). Anisotropy beneath a highly extended continental rift. *Geochemistry, Geophysics, Geosystems*, *15*, 545–564. https://doi.org/10.1002/2013GC005092

Ellis, S. M., Little, T. A., Wallace, L. M., Hacker, B. R., & Buiter, S. J. H. (2011). Feedback between rifting and diapirism can exhume ultrahigh-pressure rocks. *Earth and Planetary Science Letters*, *311*(3–4), 427–438. https://doi.org/10.1016/j.epsl.2011.09.031

Ferris, A., Abers, G. A., Zelt, B., Taylor, B., & Roecker, S. (2006). Crustal structure across the transition from rifting to spreading: The Woodlark rift system of Papua New Guinea. *Geophysical Journal International*, *166*, 622–634. https://doi.org/10.1111/j.1365-246X.2006.02970.x

Fitz, G., & Mann, P. (2013). Tectonic uplift mechanism of the Goodenough and Fergusson Island gneiss domes, eastern Papua New Guinea: Constraints from seismic reflection and well data. *Geochemistry, Geophysics, Geosystems*, *14*(10), 3969–3995. https://doi.org/10.1002/ggge.20208

Gao, S., Davis, P. M., Liu, H., Slack, P. D., Zorin, Y. A., Mordvinova, V. V., et al. (1994). Seismic anisotropy and mantle flow beneath the Baikal rift zone. *Nature*, *371*, 149–151. https://doi.org/10.1038/371149a0

Göğüş, O. H., Pysklywec, R. N., Şengör, A. M. C., & Gün, E. (2017). Drip tectonics and the enigmatic uplift of the central Anatolian Plateau. *Nature Communications*, *8*(1), 1538. https://doi.org/10.1038/s41467-017-01611-3

Gordon, S. M., Little, T. A., Hacker, B. R., Bowring, S. A., Baldwin, S. L., & Kylander-Clark, A. R. C. (2012). Multi-stage exhumation of young UHP–HP rocks: Timescales of melt crystallization in the D'Entrecasteaux Islands, southeastern Papua New Guinea. *Earth and Planetary Science Letters*, *351–352*, 237–246. https://doi.org/10.1016/j.epsl.2012.07.014

Hall, R. (2002). Cenozoic geological and plate tectonic evolution of SE Asia and the SW pacific: Computer-based reconstructions, model and animations. *Journal of Asian Earth Sciences*, *20*(4), 353–431. https://doi.org/10.1016/S1367-9120(01)00069-4

Haschke, M., & Ben-Avraham, Z. (2005). Adakites from collision-modified lithosphere. *Geophysical Research Letters*, *32*(15), L15302. https://doi.org/10.1029/2005GL023468

Holm, R. J., Spandler, C., & Richards, S. W. (2015). Continental collision, orogenesis and arc magmatism of the Miocene Maramuni arc, Papua New Guinea. *Gondwana Research*, *28*(3), 1117–1136. https://doi.org/10.1016/j.gr.2014.09.011

Huang, Z., Zhao, D., & Liu, X. (2015). On the trade-off between seismic anisotropy and heterogeneity: Numerical simulations and application to Northeast Japan. *Journal of Geophysical Research: Solid Earth*, *120*(5), 3255–3277. https://doi.org/10.1002/2014JB011784

Jin, G., Gaherty, J. B., Abers, G. A., Kim, Y., Eilon, Z., & Buck, W. R. (2015). Crust and upper mantle structure associated with extension in the Woodlark Rift, Papua New Guinea from Rayleigh-wave tomography. *Geochemistry, Geophysics, Geosystems*, *16*(11), 3808–3824. https://doi.org/10.1002/2015GC005840

Kennett, B., & Engdahl, E. R. (1991). Traveltimes for global earthquake location and phase identification. *Geophysical Journal International*, *105*(2), 429–465. https://doi.org/10.1111/j.1365-246X.1991.tb06724.x

Kennett, B. L. N., & Davies, D. R. (2020). Intra-plate volcanism in North Queensland and eastern New Guinea: A cryptic mantle plume? *Gondwana Research*, *79*, 209–216. https://doi.org/10.1016/j.gr.2019.10.003

Kington, J. D., & Goodliffe, A. M. (2008). Plate motions and continental extension at the rifting to spreading transition in Woodlark basin, Papua New Guinea: Can oceanic plate kinematics be extended into continental rifts? *Tectonophysics*, *458*(1–4), 82–95. https://doi.org/10.1016/j.tecto.2007.11.027

Laske, G., Masters, G., Ma, Z. T., & Pasyanos, M. (2013). Update on CRUST1.0—A 1-degree global model of Earth's crust. *Geophysical Research Abstracts*, *15*. Abstract EGU2013-2658.

Little, T. A., Hacker, B. R., Gordon, S. M., Baldwin, S. L., Fitzgerald, P. G., Ellis, S., & Korchinski, M. (2011). Diapiric exhumation of Earth's youngest (UHP) eclogites in the gneiss domes of the D'Entrecasteaux Islands, Papua New Guinea. *Tectonophysics*, *510*(1–2), 39–68. https://doi.org/10.1016/j.tecto.2011.06.006

Lus, W. Y., McDougall, I., & Davies, H. L. (2004). Age of the metamorphic sole of the papuan ultramafic belt ophiolite, Papua New Guinea. *Tectonophysics*, *392*, 85–101. https://doi.org/10.1016/j.tecto.2004.04.009

Martinez, F., & Taylor, B. (1996). Backarc spreading, rifting, and microplate rotation, between transform faults in the Manus Basin. *Marine Geophysical Researches*, *18*(2–4), 203–224. https://doi.org/10.1007/BF00286078

Martinez, F., Taylor, B., & Goodliffe, A. (2001). Metamorphic core complex formation by density inversion and lower crust extrusion. *Nature*, *411*, 930–934. https://doi.org/10.1038/35082042

Mondy, L. S., Rey, P. F., Duclaux, G., & Moresi, L. (2018). The role of asthenospheric flow during rift propagation and breakup. *Geology*, *46*(2), 103–106. https://doi.org/10.1130/G39674.1

Monteleone, B. D., Baldwin, S. L., Webb, L. E., Fitzgerald, P. G., Grove, M., & Schmitt, A. K. (2007). Late miocene–pliocene eclogite facies metamorphism, D'Entrecasteaux Islands, SE Papua New Guinea. *Journal of Metamorphic Geology*, *25*(2), 245–265. https://doi.org/10.1111/j.1525-1314.2006.00685.x

Paige, C. C., & Saunders, M. A. (1982). LSQR—An algorithm for sparse linear equations and sparse least-squares. *ACM Transactions on Mathematical Software*, *8*, 43–71. https://doi.org/10.1145/355984.355989

Pigram, C. J., Davies, P. J., Feary, D. A., & Symonds, P. A. (1989). Tectonic controls on carbonate platform evolution in southern Papua New Guinea: Passive margin to foreland basin. *Geology*, *17*(3), 199–202. https://doi.org/10.1130/0091-7613(1989)017<0199:tcocpe>2.3.co;2

Priestley, K., Ho, T., & McKenzie, D. (2021). The formation of continental roots. *Geology*, *49*(2), 190–194. https://doi.org/10.1130/G47696.1

Sengör, A. M. C., & Burke, K. (1978). Relative timing of rifting and volcanism on Earth and its tectonic implications. *Geophysical Research Letters*, *5*, 419–421. https://doi.org/10.1029/GL005i006p00419

Silver, P. G. (1996). Seismic anisotropy beneath the continents: Probing the depths of geology. *Annual Review of Earth and Planetary Sciences*, *24*, 385–432. https://doi.org/10.1146/annurev.earth.24.1.385

Smith, I. E. M., & Davies, H. L. (1976). Geology of the southeast Papuan mainland. *BMR Journal of Australian Geology and Geophysics*, *165*, 86.

Stolz, A. J., Davies, G. R., Crawford, A. J., & Smith, I. E. M. (1993). Sr, Nd and Pb isotopic compositions of calc-alkaline and peralkaline silicic volcanics from the D'Entrecasteaux Islands, Papua New Guinea, and their tectonic significance. *Mineralogy and Petrology*, *47*(2–4), 103–126.

Taylor, B., Goodliffe, A. M., & Martinez, F. (1999). How continents break up: Insights from Papua New Guinea. *Journal of Geophysical Research*, *104*, 7497–7512. https://doi.org/10.1029/1998JB900115

Taylor, B., & Huchon, P. (2002). Active continental extension in the western Woodlark basin: A synthesis of leg 180 results. In P. Huchon, B. Taylor, & A. Klaus (Eds.), *Proceedings of the ocean drilling program, scientific results* (Vol. 180, pp. 1–36). Ocean Drilling Program. https://doi.org/10.2973/odp.proc.sr.180.150.2002

Tregoning, P., Lambeck, K., Stolz, A., Morgan, P., McClusky, S. C., van der Beek, P., et al. (1998). Estimation of current plate motions in Papua New Guinea from Global Positioning System observations. *Journal of Geophysical Research*, *103*(B6), 12181–12203. https://doi.org/10.1029/97JB03676

Van Wijk, J. W., & Blackman, D. K. (2005). Dynamics of continental rift propagation: The end-member modes. *Earth and Planetary Science Letters*, *229*(3–4), 247–258. https://doi.org/10.1016/j.epsl.2004.10.039

Wallace, L. M., Ellis, S., Little, T., Tregoning, P., Palmer, N., Rosa, R., et al. (2014). Continental breakup and UHP rock exhumation in action: GPS results from the Woodlark Rift, Papua New Guinea. *Geochemistry, Geophysics, Geosystems*, *15*(11), 4267–4290. https://doi.org/10.1002/2014GC005458

Wallace, L. M., Stevens, C., Silver, E., McCaffrey, R., Loratung, W., Hasiata, S., et al. (2004). GPS and seismological constraints on active tectonics and arc-continent collision in Papua New Guinea: Implications for mechanics of microplate rotations in a plate boundary zone. *Journal of Geophysical Research: Solid Earth*, *109*(B5), B05404. https://doi.org/10.1029/2003JB002481

Wang, J., & Zhao, D. (2013). P-wave tomography for 3-D radial and azimuthal anisotropy of Tohoku and Kyushu subduction zones. *Geophysical Journal International*, *193*(3), 1166–1181. https://doi.org/10.1093/gji/ggt086

Webb, L. E., Baldwin, S. L., & Fitzgerald, P. G. (2014). The early-middle Miocene subduction complex of the louisiade archipelago, southern margin of the Woodlark rift. *Geochemistry, Geophysics, Geosystems*, *15*(10), 4024–4046. https://doi.org/10.1002/2014GC005500

Webb, L. E., Baldwin, S. L., Little, T. A., & Fitzgerald, P. G. (2008). Can microplate rotation drive subduction inversion? *Geology*, *36*, 823–826. https://doi.org/10.1130/G25134A.1

Weissel, J. K., Taylor, B., & Karner, G. D. (1982). The opening of the Woodlark Basin, subduction of the Woodlark spreading system, and the evolution of northern Melanesia since mid-Pliocene time. *Tectonophysics*, *87*(1–4), 253–277. https://doi.org/10.1016/0040-1951(82)90229-3

West, J. D., Fouch, M. J., Roth, J. B., & Elkins-Tanton, L. T. (2009). Vertical mantle flow associated with a lithospheric drip beneath the Great Basin. *Nature Geoscience*, *2*(6), 439–444. https://doi.org/10.1038/ngeo526

Westaway, R. (2005). Active low-angle normal faulting in the Woodlark extensional province, Papua New Guinea: A physical model. *Tectonics*, *24*(6), TC6003. https://doi.org/10.1029/2004TC001744

Yu, Y., Gao, S. S., Zhao, D., & Liu, K. H. (2020). Mantle structure and flow beneath an early-stage continental rift: Constraints from P wave anisotropic tomography. *Tectonics*, *39*(2), e2019TC005590. https://doi.org/10.1029/2019TC005590

Yu, Y., Liu, K. H., Huang, Z., Zhao, D., Reed, C. A., Moidaki, M., et al. (2017). Mantle structure beneath the incipient Okavango rift zone in southern Africa. *Geosphere*, *13*(1), 102–111. https://doi.org/10.1130/GES01331.1

Yu, Y., & Zhao, D. (2018). Lithospheric deformation and asthenospheric flow associated with the Isabella anomaly in Southern California. *Journal of Geophysical Research: Solid Earth*, *123*, 8842–8857. https://doi.org/10.1029/2018JB015873

Zhang, H., Zhao, D., Yu, C., & Zhao, J. (2016). Varying deformation patterns in central Tibet revealed by radial anisotropy tomography. *Journal of Geophysical Research: Solid Earth*, *121*, 3445–3461. https://doi.org/10.1002/2016JB012832

Zhao, D., Hasegawa, A., & Horiuchi, S. (1992). Tomographic imaging of P and S wave velocity structure beneath northeastern Japan. *Journal of Geophysical Research*, *97*, 19909–19928. https://doi.org/10.1029/92JB00603

Zhao, D., Hasegawa, A., & Kanamori, H. (1994). Deep structure of Japan subduction zone as derived from local, regional, and teleseismic events. *Journal of Geophysical Research*, *99*, 22313–22329. https://doi.org/10.1029/94JB01149